Stiffness measurement system using endoscopes with a visualization method

Tetsuyou Watanabe, Member, IEEE, Takanobu Iwai, Toshio Koyama, and Takeshi Yoneyama

***Abstract*—A novel stiffness-sensing system was developed that works by attaching the proposed sensing part to endoscopes or cameras. The system provides a method to investigate the stiffness of tissues or objects in deep areas that can only be observed with endoscopes in order to detect abnormalities. The system is an extension of our previous force sensing system that utilized a force visualization mechanism. The force is visualized at the sensing part, and can be measured as visual information via endoscopes or cameras. The sensing part also has a limiting structure used as a threshold for the applied force. By measuring the force at the limitation, the stiffness can be measured. The limitation point is detected by the brightness changes of the captured images. The developed sensing part has the advantages of having no electronic components, being disposable, simple, easy to sterilize, MRI-compatible, and low-cost. Image processing methods for realizing the mechanism are also proposed. The system was experimentally validated.**

***Index Terms*—Force sensors; Endoscopes; Stiffness sensors; Force visualization method**

I. Introduction

ENDOSCOPES are powerful instruments that enable visualization of areas that people cannot enter or touch directly. In the medical field, endoscopes are widely used for invasive examinations. They are used not only for medical checks, but also in surgeries. Endoscopes are also useful for detecting faults inside machines. However, they typically provide only visual information. If operators and doctors could access not only visual, but also haptic information, then more accurate diagnoses could be made. For example, palpation is a frequently used diagnostic method in small hospitals and clinics. The tactile information during abdominal surgery can be used to detect the difference between normal and malignant tissues. Tightening of screws could be achieved if tactile information was available. With this in mind, in our previous papers [1], [2], we developed a force sensing system that can be attached to fiberscopes or endoscopes. Its main applications fell within the field of medicine. Utilizing a highly elastic material (panty stocking fabric) to create a force visualization mechanism results in a force sensing system with high resolution, small size, low cost, no electrical components, and disposable parts. However, the functions required to detect afflicted tissue areas include not only force measurements, but also stiffness or softness of the tissue. A similar analogy can be observed in other fields such as factories and plants. Therefore, this paper presents a novel stiffness-sensing system that works by attaching a force sensing component to an endoscope to detect abnormalities. The main features are as follows:

- **Visualization mechanism-based sensing system**: The developed stiffness-sensing system is an extension of our force sensing system [1], [2]. The sensing system was completed by appending the sensing part to the end of endoscopes or cameras. The force or displacement of the sensing part is visualized using the scope, and converted into force and stiffness measurements. The sensing part has the advantages of having no electrical components, being disposable, a simple design, easy sterilization, MRI-compatibility, and low-cost.
- **Mechanical structure for limiting the applied force**: The sensing part has a structure used to limit the encountered force. By measuring the force at this limitation, the stiffness can be determined.
- **Strategy for detecting the force limitation**: The change in brightness of the image is used to detect the force limitation. The light source is located outside of the sensing part. The limiting structure also works to block the light. Therefore, if the brightness substantially decreases, it indicates the applied force has met the structural limitations of the system. Through detecting this change, the point for measuring stiffness is obtained.

This paper also proposes new image processing methodologies to realize mechanisms that include these features.

Our previous conference paper [3] provides a summarized description of the concept used in this sensing system. However, the strategy for detecting the force limitation was unclear. Therefore, this paper presents the strategy to detect force limitations used to determine stiffness, in addition to the structural modifications to the sensing part required for implementation of the strategy.

After introducing related works, this paper is organized as

An earlier version of this paper was presented at the IEEE EMBC Conference and was published in its Proceedings http://ieeexplore.ieee.org/xpl/articleDetails.jsp?arnumber=7319869. This work was supported by JSPS KAKENHI Grant Number 16H04298.

T. Iwai and T Koyama are with the Department of mechanical Engineering, College of science and engineering, Kanazawa University, Ishikawa, Japan.

T. Yoneyama and T. Watanabe are with the Institute of Science and Engineering, Kanazawa University, Kakuma-machi, Kanazawa, 9201192, Japan (e-mail: yoneyama@t.kanazawa-u.ac.jp; te-watanabe@ieee.org). (corresponding author to provide e-mail: te-watanabe@ieee.org)

follows. First, the main structure and principle are described. Second, the strategy for detecting the force limitation is presented. After describing how to derive the force and displacement information from the visual information, the experimental validations are shown. Lastly, the conclusion is presented.

A. Related works

Many force and tactile sensors have been developed. Dahiya et al. presented a detailed review for tactile sensors [4]. Tiwana et al. reviewed tactile sensors in the biomedical field [5]. The presented sensing system in this paper works with endoscopes. Force and tactile sensors have wide applications in the medical field. Primarily, the sensors are used to provide tactile feedback to a medical doctor or an operator. Puangmali et al. [6], Westebring et al. [7], Okamura [7], and Poorten et al. [8] presented reviews for this type of haptic technology.

Most of the haptic feedback systems used for minimally invasive robotic surgery require electronic components such as strain gauges [9]–[11]. However, electrical devices are not always preferable in the medical field. The electrical force gauge and tactile sensors often require other devices, such as amplifiers, to function, resulting in increased total costs and large-sized systems. Difficulties in sterilizing or disinfecting are also common problems. With this in mind, several sensor systems without electronic components have been developed. Takaki et al. developed a force sensor embedded in forceps by utilizing moiré fringe patterns [12]. The group of Kawashima developed a pneumatic force sensing system embedded in pneumatically driven forceps [13], [14]. Peirs et al. developed a force sensor utilizing optical fibers to visualize the deformation of a flexible structure embedded in the sensor [15]. Tada et al. developed a force sensor that detects peak illumination changes of a point light source attached to a flexible structure [16]. Ohka et al. developed a three-axis force sensor that detects the position and orientation of columnar and conical markers by cameras, which changes depending on the applied force [17]. Kamiyama et al. developed a sensor that can estimate the magnitude, distribution, and direction by detecting the motion of two layered markers with cameras [18]. Chorley et al. developed a biologically inspired vision-based tactile sensor (TACTIP) [19].

With regarding to stiffness sensors, Kawahara et al. developed a stiffness measuring system that supplies air streams to a target and captures the deformation caused by the air pressure by using endoscopes or cameras [20]. The drawback of this system is its complexity and large size. Fukuda et al. developed a sensing system that detects the softness of tissue via acoustic reflection [21]. However, only relative comparison is available, and quantitative values of stiffness cannot be obtained. Although there are some types of stiffness sensing systems, their development is limited, and still have many unresolved problems. Therefore, this paper aims to develop a low-cost and simple stiffness-sensing system.

II. STRUCTURE AND PRINCIPLE

Fig. 1 shows the overview of the developed stiffness-sensing system. The system consists of a sensing part, an endoscope or camera, a light source, and a PC. If the sensing part makes contact with an object, the image change associated with the force/load and subsequent displacement is captured by the camera (contained within the endoscope), and analyzed by a PC. The sensing part has a structure that acts as a force limit, and by sensing the force at this limit, the stiffness information of the object can be obtained.

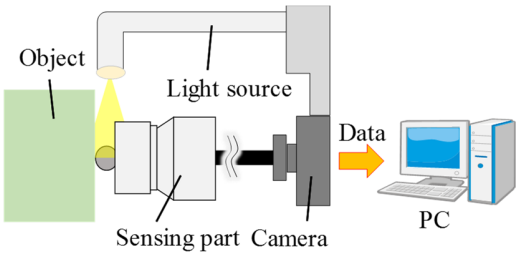

Fig. 1. Schematic view of the proposed stiffness-sensing system.

Here, we define stiffness. Let f[N] be the force/load applied to the object by the sensing part, and x [mm] be the deformation of the object, as shown in Fig. 2. The stiffness is defined as follows

$$\text{stiffness} = \frac{f}{x}\ [\text{N/mm}] \qquad (1)$$

Note that the stiffness given in (1) was used rather than the elastic modulus in order to take future applications to haptic feedback systems into account.

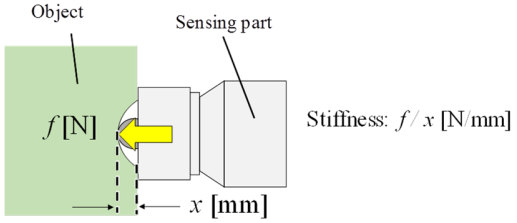

Fig. 2. Schematic of stiffness.

A. Structure of sensing part

Fig. 3 shows the (a) overview, (b) photo, (c) side view, and (d) cross-sectional view of the proposed sensing part. The sensing part is composed of a pin, a limiting component, a silicon part, and main body part, as shown in Fig. 4. These four parts are connected with a fitting. The silicone part played a key role acting as a spring, and was made of silicone: KE-1308 and hardener (volume: 6 %): CAT1300L-3 (Shin-etsu Silicone, see [22], [23] for details on the stiffness information; Fig. 17 (a) shows the material information for the relationship between the load and displacement). Note that the viscosity of this material (silicone) has negligible difference compared to other polymer materials (e.g., [24]). This is one reason why this material was chosen. The silicone part was transparent so that the light source could transmit through the sensing part. The pin, limiting component, and main body part (ABS plus: Young's Modulus: 2.2 [GPa]) were manufactured by a 3D printer (Stratasys Uprint SE). The pin had a spherical-shaped head and a cylindrical extension. The pin head was a sphere having a diameter of 8 [mm]. It was designed such that the distance between the top of

the pin and the limiting component (l_0) was 7 [mm] when the pin reached the limitation of displacement, as shown Fig. 3 (d). p_c is defined as the point at which the pin reaches the limit. It should be noted that the distance between the top of the pin and the limiting component (l_0) was set as 7 [mm]; however, because of a manufacturing and processing error, $l_0 = 7$ was not always convenient. Therefore, l_0 was used to represent this distance in the later discussion.

Fig. 5 shows a schematic of the pins making initial contact with an object (left side) and reaching their limitation point p_c (right side). Fig. 5 also shows the corresponding images captured at these stages. When the pin head makes contact with an object or organ, the silicone part deforms, and the pin displaces based on the deformation. By capturing the displacement of the pin via camera, force or displacement can be estimated.

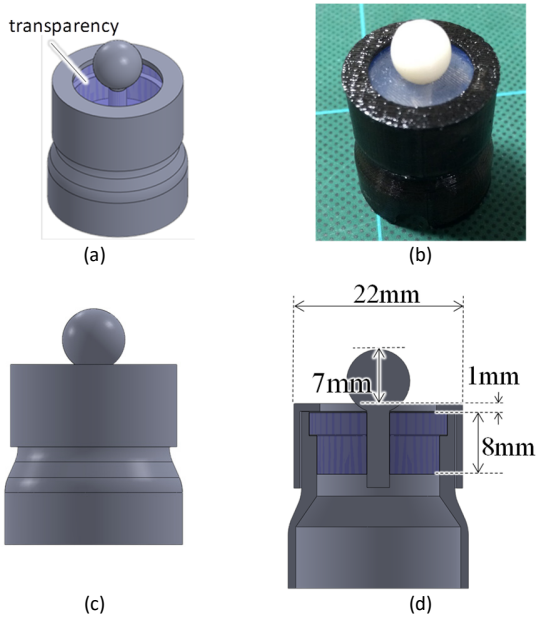

Fig. 3. The proposed sensing part (a) overview; (b) photo; (c) side view; (d) cross-sectional view

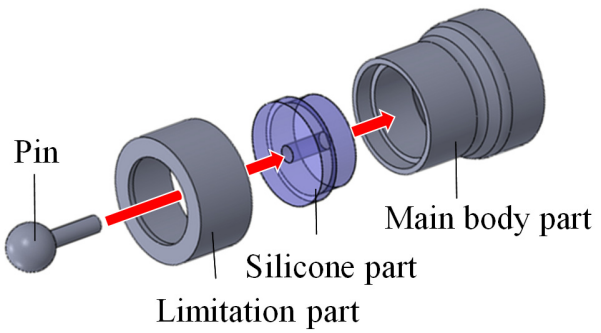

Fig. 4. The components of the sensing part

B. *Principle for stiffness estimation*

Let l be the displacement of the pin as shown in Fig. 5. Here, consider the case when the pin reaches its limit p_c. In this case, the relationship between the displacement of the pin l [mm] and the deformation of the object x [mm] is represented by

$$l + x = l_0\ [mm] \tag{2}$$

Therefore, if l and f at the limitation point p_c can be obtained, then the stiffness given in (1) can be calculated utilizing (2). In sum, the necessary information for stiffness estimation is as follows:

1. Detection of the limit p_c
2. Estimation of the displacement l and the load f at p_c

1) Detection of the limitation point p_c

A light source is assumed to be located outside the sensing part. When the images at the initial state (where the pin head initially contacts the object) and limitation point p_c (see Fig. 5) are compared, it can be seen that the brightness clearly differs. This is due to the difference in the transmissivity of light from the light source. The yellow arrows in Fig. 5 describe a model of this principle. At the initial state, there is space for light transmission. Because of the transparency of the silicone, the light can easily transmit inside the sensing part, and an image having high brightness can be obtained. On the other hand, at the limitation point p_c, the object covers the limitation structure and there is little space for light transmission. The amount of light that can transmit through the sensing part then decreases significantly. Therefore, we get an image with low brightness. By detecting the change in the brightness, the limitation point p_c can be obtained.

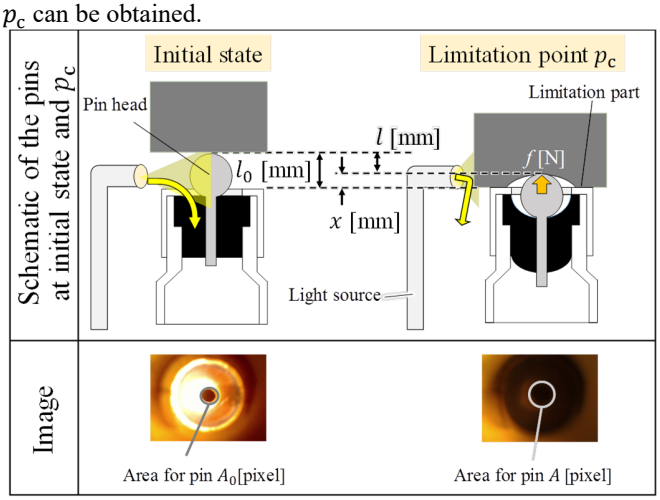

Fig. 5 Schematic of the pins making initial contact with an object (left side) and reaching their limitation point p_c (right side), and the corresponding images captured at these stages.

2) Estimation of the displacement l and the load f at the limitation point p_c

Load f [N] and the displacement l [mm] can be estimated by the same strategy as presented in our previous works [1]–[3], although different image processing methods are required to realize the strategy because of the different brightness conditions. If a load f is applied to the pin head, then the pin displaces based on the deformation of the silicone part. The captured area for the pin changes from A_0 (initial area without load) to A, as seen in Fig. 5. Therefore, the load f can be derived from $A - A_0$ if we know the relation between f and $A - A_0$. Note that the relation includes the nonlinear elastic

property of the silicone part at the sensing part. By a similar method, l can also be estimated. Note that the three-axis force can theoretically be measured as proposed in a previous study [2]. The main purpose in this paper pertains to the estimation of stiffness, specifically in the longitudinal direction of the pin.

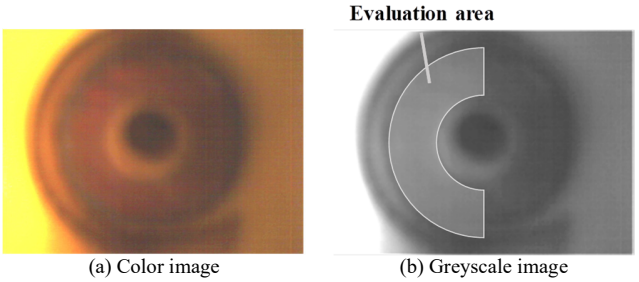

(a) Color image (b) Greyscale image

Fig. 6 Evaluation area for detecting the limitation point p_c; (a) the captured color image, (b) converted greyscale image highlighting the evaluation area

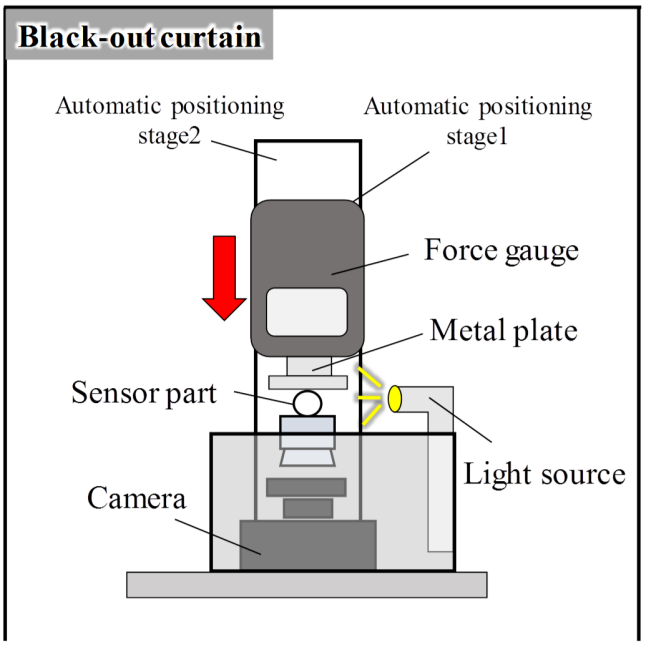

Fig. 7 Schematic view of the experimental setup

III. Procedure for Detecting the Limitation Point p_c

When the brightness of the captured image is lower than the threshold, it signifies that the pin head has reached the limitation point p_c. The key factors involved in applying this method include the area for brightness evaluation and the threshold. The brightness of the captured image is not uniform because of the position of light source. As shown in Fig. 5, the light source was located such that the light came from the right and transmitted towards the left. Therefore, a relatively large change in brightness could be obtained in the left half of the resulting image. If evaluating both left and right areas of an image, the change in brightness could be unclear. Additionally, there was little change in the brightness around pin. Therefore, we defined the evaluation area to be that shown in Fig. 6. The evaluation area was constructed by subtracting a smaller left semi-circle area (radius: 80 [pixel]) from a larger semi-circle area (radius: 160 [pixel]) so that the change in brightness could be clear. The centers for both semicircles coincided with the center of the pin. The procedure for the evaluation was as follows:

1. The captured image was converted to a grayscale image.
2. The mean of the pixel values in the evaluation area (P) was calculated.

The obtained P value was the target for evaluating the brightness. The threshold for detecting the limitation point $p_c$was experimentally derived.

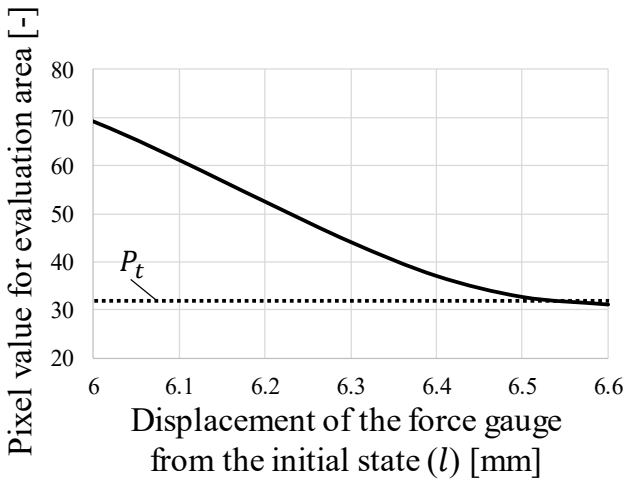

Fig. 8. Relationship between the pixel value for the evaluation area and the displacement of the force gauge from the initial state (l).

A. Experiment for determining the threshold

Fig. 7 shows a schematic view of the experimental setup. The sensing part was attached to the camera (Elecom UCAM-DLT30HSV: resolution: 640×480 [pixel]). Note that here the camera was used instead of the endoscope to simplify the setup. A force gauge (IMADA DS2-500N) was attached to the automatic positioning stage 1 (SIGMAKOKI TAMM40-10C). The flat plate was attached to the tip of the force gauge. The automatic positioning stage 1 was also attached to the automatic positioning stage 2 (IMADA MX2-500N). The role of automatic positioning stage 1 was precise motion, while the role of automatic positioning stage 2 was large motion. A black-out curtain was used to block the ambient light in order to isolate the light from the light source (MITSUTOYO Megalight100) located to the right of the sensing part. The force gauge was adjusted until the pin head of the developed sensing part was pressed up to the flat plate. Initially, the force gauge was set to a value of 0.00 [N] when the plate just barely contacted the sensing part. Then, the automatic positioning stages were controlled to increase the displacement by increments of 1.00 [mm], until the total displacement reached 6.00 [mm]. After that, the displacement increased by increments of 0.10 [mm] until the total displacement reached 6.60 [mm]. It should be noted that when the total displacement reached 6.60 [mm], a sudden and substantial increase in load was observed. At this point, we stopped increasing the displacement. This indicated that the contact between the limiting structure and the plate occurred when the total displacement changed from 6.50 to 6.60

[mm]. At each step, the value of the force gauge and the moving distance of the automatic positioning stage (l) were recorded, and a photo was taken with the camera. These experimental results were used not only to determine the deviation of the threshold for detecting the structural limitation but also for estimating the load f and the displacement l from the image of pin.

Let P_t be the pixel value for the evaluation area at the limitation point p_c. Here, we tried to derive not only the threshold P_t but also l_0 (the distance between the top of the pin and the limiting part), taking the manufacturing and processing errors into account. For this, we used the data from when the total displacement went from 6.00 to 6.60 [mm]. Fig. 8 shows the obtained relationship between the pixel value for the evaluation area and the displacement of the force gauge from the initial state (l). It was confirmed that the contact between the limiting structure and the plate occurred when the total displacement went from 6.50 to 6.60 [mm]. The corresponding pixel values for the evaluation area were $P = 32.8$ at 6.50 [mm] and $P = 31.2$ at 6.60 [mm]. We set $P_t = 32$ to be the threshold value for detecting the limitation point p_c. Additionally we set $l_0 = 6.50$ [mm] in (1). Note that this value was different from the designed value 7 [mm] (see Fig. 3 (d)). This was due to manufacturing and processing errors.

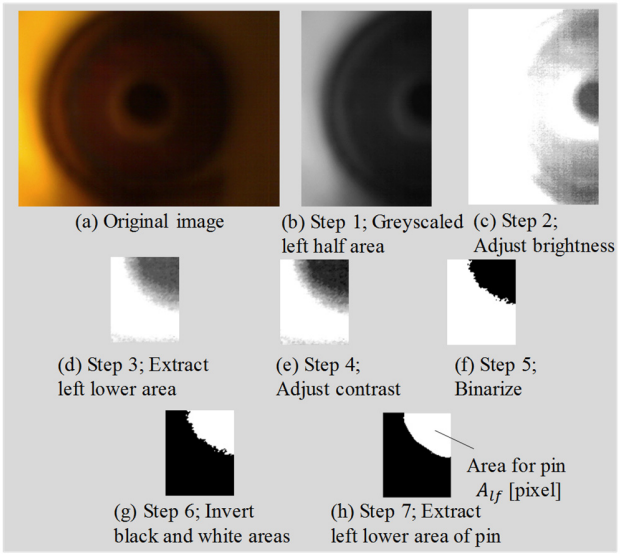

Fig. 9 Procedure for deriving the left lower area for pin (A_{lf}).

IV. Procedure for Estimating the Load f and the Displacement l

Because the difference in the area of the pin from its initial sate, $A - A_0$, corresponds to a load f and a displacement l, we considered deriving the relationship between $A - A_0$ and f (l). However, as mentioned the above, the image around pin is not uniform because of the position of light source. Therefore, we derived the left lower area for pin A_{lf} instead of A, because the left lower area for pin was relatively stable and uniform. We then used the relationship between $A_{lf} - A_{lf0}$ and f (l), letting A_{lf0} be A_{lf} represent the initial state. The left lower area for the pin is a quarter circle, so $A_{lf} - A_{lf0} = (A - A_0)/4$. As shown in Fig. 5, the target image (at the limitation point p_c) was dark and is not easy to derive the area of the pin. A method that employs another light source located inside the sensing part, could potentially be used. However, the ability to derive the area of the pin from the dark image, would enable construction of a simpler system. Therefore, we challenged the problem by using the following algorithm (see Fig. 9):

Step 1. Convert to greyscale image and cut the right half area of pin.
Step 2. Adjust brightness.
Step 3. Extract the area including left lower area for pin.
Step 4. Adjust contrast
Step 5. Binarize
Step 6. Invert black and white areas
Step 7. Make the boundary clear and extract left lower area of pin

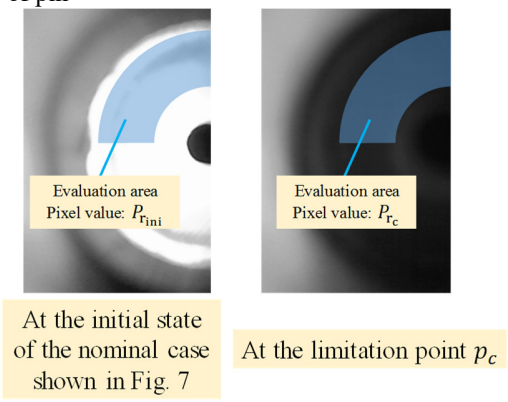

Fig. 10. The evaluation areas for the brightness adjustment.

At Step 1, as a preprocessing step for extracting the left lower area for pin, the color image was converted to a greyscale image. The right half of the image was cut, but the left upper area was not cut because it was used for brightness adjustment.

In order to extract a quarter circle area for the pin from a dark image, we conducted two-step adjustments. In the first step, we adjusted the brightness. In Step 2, we defined the reference pixel value P_r for the brightness adjustment. The purpose of this adjustment was to increase the total brightness of the image and to remove the effects of shadows. P_r was set to be the mean pixel value of the evaluation area where the shadow effect was strong, as shown in Fig. 10 (left upper arced area with a radius from 80 to 160 [pixel]). Let $P_{r_{ini}}$ and P_{r_c} be the P_r at the initial state of the nominal case shown in Fig. 7 and the limitation point p_c. In order to let $P_{r_{ini}}$ be the constant stable value, we used P_r at the initial state of the nominal case (when contacting flat plate) shown in Fig. 7. Let $I_{1x,y}$ be the image pixel value at the point $(x, y)^T$ of the image after Step 1, and $I_{2x,y}$ be the image pixel value after the brightness adjustment. Then,

$$I_{2x,y} = \min\left(255, \min(R_{max}, \frac{P_{r_{ini}}}{P_{r_c}})I_{1x,y}\right) \quad (3)$$

where R_{max} is the specified value used to prevent the brightness from being too high. We set $R_{max} = 9$ when P_r at the initial state was over 210 and $R_{max} = 8$ when it was under 210.

After cutting the left upper area of the pin in Step 3, we

adjusted the contrast in Step 4, in order to make the boundary of area for pin clear. Letting $I_{3x,y}$ be the image pixel value after Step 3, and $I_{4x,y}$ be the image pixel value after the contrast adjustment, we used the following equation:

$$I_{4x,y} = \min\left(255, \frac{255}{C_{high} - C_{low}} I_{3\min x,y}\right) \quad (4)$$
$$I_{3\min x,y} = \max(0, I_{3x,y} - C_{low})$$

where

$$C_{low} = \min_{x,y} I_{3x,y}$$

Here, C_{low} and C_{high} ($C_{high} \geq C_{low}$) represent the range for adjustment, corresponding to 0 and 255 in the adjusted image, respectively. We set $C_{high} = 240$ in this study.

After the contrast adjustment, binarization was conducted in Step 5, utilizing a modified Otsu method [25]. We took into account only pixel values under 230 in the Otsu method [25]. In Step 6, the image was inverted to get the information of the area of the pin. Finally, in Step 7, we extracted the left lower area for pin after making the boundary clear by computing the convex hull of the area.

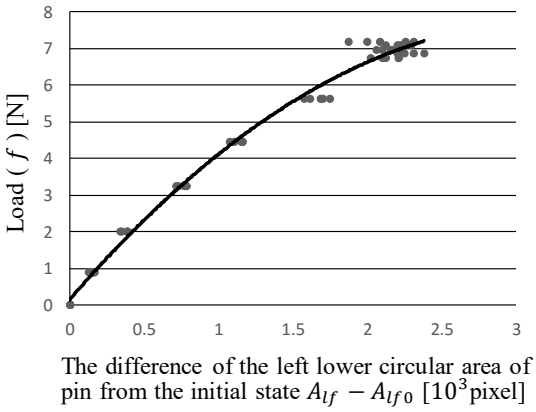

Fig. 11. Relationship between the difference of the left lower circular area of the pin from the initial state $A_{lf} - A_{lf0}$ and the load f.

A. Relationship between the area for pin and the load f (the displacement l)

We used the data obtained from the experiments described in the previous section to get the relationship between the load f (the displacement l), and the difference of the left lower circular area of the pin from the initial state, $A_{lf} - A_{lf0}$. $A_{lf} - A_{lf0}$ was derived by the method described above. Fig. 11 shows the relationship between $A_{lf} - A_{lf0}$ and the load f, while Fig. 12 shows the relationship between $A_{lf} - A_{lf0}$ and the displacement l.

For the relationship between $A_{lf} - A_{lf0}$ and the load f, the following regression curve was used:

$$f = a_2(A_{lf} - A_{lf0})^2 + a_1(A_{lf} - A_{lf0}) + a_0 \quad (5)$$

where $a_2 = -0.726$, $a_1 = 4.69$, and $a_0 = 0.151$. The coefficient of determination was 0.99. It can be seen that the regression curve represented the relationship very well.

For the relationship between $A_{lf} - A_{lf0}$ and the displacement l, the following regression curve was used:

$$l = b_2(A_{lf} - A_{lf0})^2 + b_1(A_{lf} - A_{lf0}) + b_0 \quad (6)$$

where $b_2 = -0.663$, $b_1 = 4.15$, and $b_0 = 0.265$. The coefficient of determination was 0.99. It can be seen that the regression curve represented the relationship very well.

Note that (5) and (6) include the nonlinear elastic property of the silicone part at the sensing part.

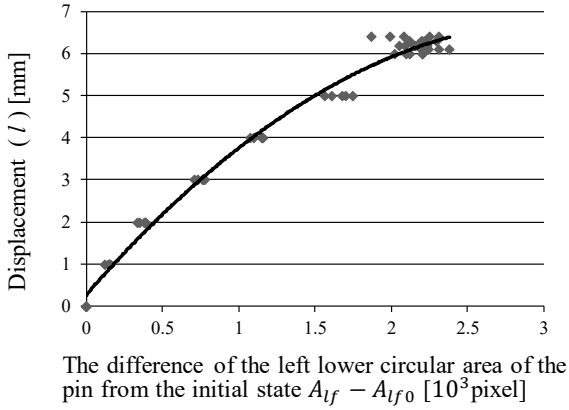

Fig. 12. Relationship between the difference of the left lower circular area of the pin from the initial state $A_{lf} - A_{lf0}$ and the displacement l.

V. Experimental Validation of Stiffness Estimation

In order to see the validity of the developed system, we conducted experiments estimating the stiffnesses of objects made of silicone (silicone: KE-1308 and hardener (volume: 6 %): CAT1300L-3, produced by Shin-etsu Silicone) and melamine. The experiment not only checks whether or not the stiffness value can be obtained but also sees whether or not the proposed sensing system can detect the difference between hard (silicone) and soft (melamine) objects, supposing abnormal and normal objects. As shown in Fig. 13, the target objects were prismatic columns with a height of 11 [mm]. The base prism was inscribed in a circle with a radius of 11 [mm]. The shape was set so that the objects could match the outside of the sensing part (see Fig. 3). Note that this setting is not a discrepancy with JIS K 6254 corresponding to ISO 7743 (Rubber, vulcanized or thermoplastic—Determination of stress-strain properties). Fig. 14 shows the schematic view of the experiment, which is the same as that shown in Fig. 7, except for the existence of a soft object between the metal plate and the sensing part. Initially, once the soft object (silicone or melamine) had just contacted the sensing part, the force value was set to 0.00 [N]. Then, the automatic positioning stages were controlled to increase the displacement by 1.00 [mm], until the total displacement reached 6.00 [mm]. After that, the automatic positioning stages were controlled to increase the displacement by 0.10 [mm], until the total displacement reached 6.60 [mm]. At each step, the value of the force gauges and the moving distance of the automatic positioning stage (l) were recorded, and a photo was taken by the camera. The experiment was repeated 5 times for each sample.

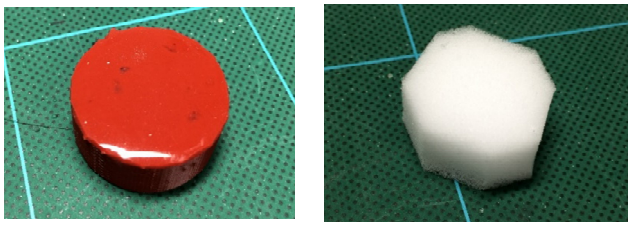

(a) (b)

Fig. 13 Photos of the target objects in the experiment; (a) silicone and (b) melamine form

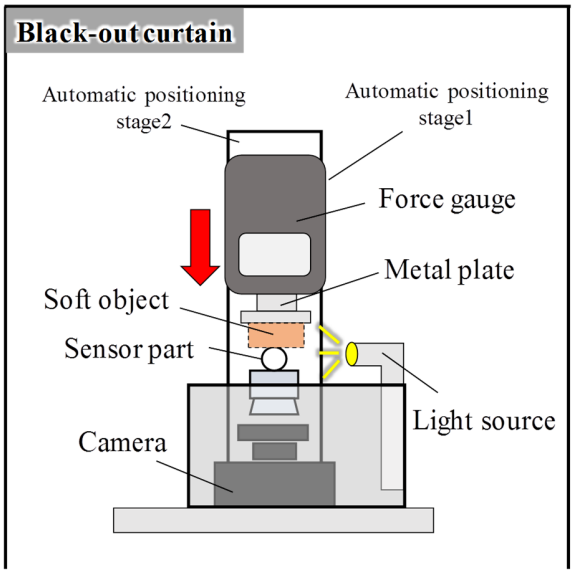

Fig. 14 Schematic view of the experimental setup for estimating the stiffnesses of objects made of silicone and melamine form.

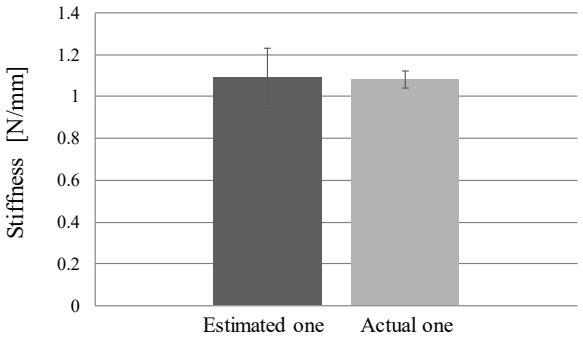

(a) Target object was silicone

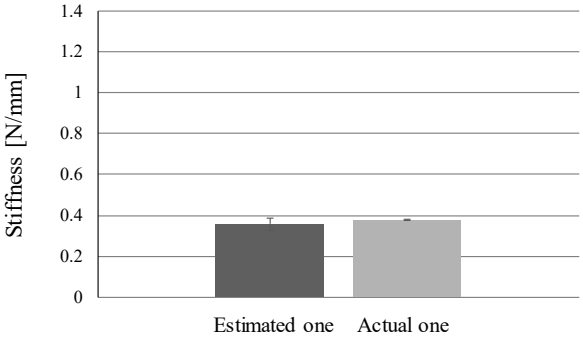

(b) Target object was melamine form

Fig. 15 Results of stiffness estimation and experimentally obtained actual stiffness values; (a) silicone and (b) melamine form

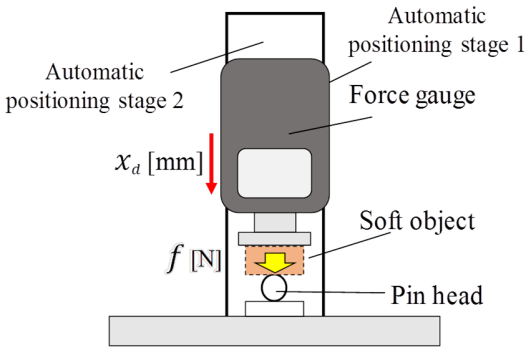

Fig. 16 Schematic view of the experimental setup for obtaining actual stiffness. The relationship between the load f and the displacement x_{d} was obtained.

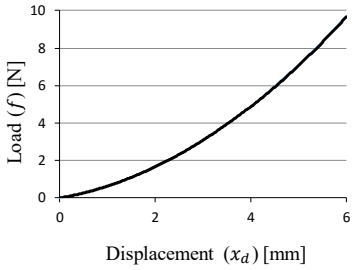

(a) Target object was silicone

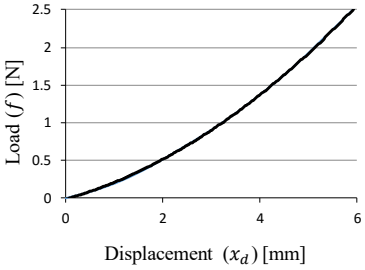

(b) Target object was melamine form

Fig. 17 The relationship between the load (f) and the displacement (x_{d}); (a) silicone and (b) melamine form.

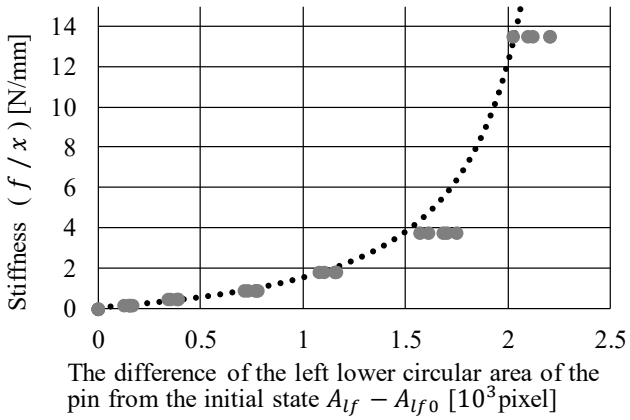

Fig. 18 The relationship between the difference of the left lower circular area of the pin from the initial state $A_{lf} - A_{lf0}$ and the stiffness f/x, with the experimental values; It indicates the resolution of the developed sensing system.

Using the previously described methods, we derived the difference of the left lower circular area of the pin from the initial state, $A_{lf} - A_{lf0}$, the load f (see (5)), and the displacement l (see (6)). Utilizing (1) and (2), we derived the

stiffness of the soft objects. The obtained results are shown in Fig. 15. For comparison, actual stiffness values are also shown.

Actual stiffness values were obtained experimentally. Fig. 16 shows the schematic view of the setup for the experiment. A sphere whose size and material were the same as the pin head was fixed to a table, instead of the sensing system. This part was different from the setup shown in Fig. 14. The other settings were the same. The procedure was also the same. Initially, the force was set to 0.00 [N] when the soft object (silicone or melamine form) just barely contacted the sphere. Then, the automatic positioning stages were controlled to increase the displacement until the total displacement reached 6.00 [mm]. The value of force gauges and the moving distance of automatic positioning stage (x_d) were recorded at an interval of 0.0083 [mm]. Fig. 17 shows the obtained relationship between the load f and the displacement x_d. Because the stiffness varied with the displacement x_d, the relationship could be obtained. In the experiment of stiffness estimation, the actual displacement (x) information was obtained. By letting x_d be x, we derived the actual and corresponding stiffness from the relationship shown in Fig. 17.

From Fig. 15, it can be seen that there was little difference between the estimated and the actual stiffness values. Although the variation for the estimated stiffness values was larger than that of the actual stiffness values, it was still small. In addition, the difference in stiffness could be detected. These results prove the validity of the developed sensing system.

From (1), (2), (5), and (6), we can obtain the relationship between the stiffness and the difference of the left lower circular area of the pin from the initial sate $A_{lf} - A_{lf0}$:

$$\frac{a_2\left(A_{lf}-A_{lf0}\right)^2+a_1\left(A_{lf}-A_{lf0}\right)+a_0}{l_0-b_2\left(A_{lf}-A_{lf0}\right)^2-b_1\left(A_{lf}-A_{lf0}\right)-b_0}\ [\mathrm{N/mm}] \qquad (7)$$

Fig. 18 shows the relationship with the experimental values. This relationship indicates the resolution of the developed sensing system. It can be seen that as the stiffness of the target increases, the resolution becomes lower. If the stiffness exceeds 12 [N/mm], it is not easy to estimate the stiffness with enough resolution. We then show the relationship for the stiffness to have a range of 0 to 15 [N/mm]. In other words, the range of the developed system is 0 to 12 [N/mm]. This means that the stiffness from 0 to 2 [N/mm] is expected to be estimated with high accuracy. This is consistent with the results shown in Fig. 15.

VI. Conclusion

This paper presented a novel stiffness-sensing system that worked by attaching a sensing part to endoscopes or cameras. The system provides a method for investigating the stiffness of tissues or objects in deep areas that can only be observed with endoscopes in order to detect abnormalities. The sensing part consisted of a pin, a limiting component, a transparent silicon, and body parts. When pressing a target object with the pin, the pin displaces based on the magnitude of load because of silicone's mechanical spring property. The area of the pin in the captured image corresponded to the load and the displacement. Therefore, the values of load and displacement could be estimated with image processing. The displacement of the pin was structurally limited by the limiting component. By estimating the load at the limiting point, the stiffness of the target object could be estimated. The limiting point was detected by a brightness change of the captured image. The light source was located outside the sensing system. Because of the transparency of the silicone, images having high brightness could be captured at the initial state of examination, and images having reduced brightness could be captured at the limiting point. By detecting the change in brightness, the limiting point was detected. An image processing methodology was also presented to realize the mechanisms. The experimental results discriminating silicone and melamine objects showed the validity of the developed system. We effectively used transparent silicone as the spring. The range and resolution depend on the material properties of the silicone. By changing the material or hardness, we would have another range or resolution for the sensing system. The sensor configuration should be compatible for attachment depending on the size of endoscopes or cameras used. Identifying various ranges and resolutions of the system, in addition to optimally sizing sensors will be part of our future works.

References

[1] T. Watanabe, T. Iwai, Y. Fujihira, L. Wakako, H. Kagawa, and T. Yoneyama, "Force Sensor Attachable to Thin Fiberscopes/Endoscopes Utilizing High Elasticity Fabric," *Sensors*, vol. 14, no. 3, pp. 5207–5220, Mar. 2014.

[2] T. Iwai, Y. Fujihira, L. Wakako, H. Kagawa, T. Yoneyama, and T. Watanabe, "Three-axis force visualizing system for fiberscopes utilizing highly elastic fabric," in *2014 IEEE/ASME International Conference on Advanced Intelligent Mechatronics*, 2014, pp. 1110–1115.

[3] T. Iwai, T. Koyama, H. Kagawa, T. Yoneyama, and T. Watanabe, "Visualization method based stiffness sensing system for endoscopes," in *2015 37th Annual International Conference of the IEEE Engineering in Medicine and Biology Society (EMBC)*, 2015, pp. 6449–6452.

[4] R. S. Dahiya, G. Metta, M. Valle, and G. Sandini, "Tactile Sensing—From Humans to Humanoids," *IEEE Trans. Robot.*, vol. 26, no. 1, pp. 1–20, Feb. 2010.

[5] M. I. Tiwana, S. J. Redmond, and N. H. Lovell, "A review of tactile sensing technologies with applications in biomedical engineering," *Sensors Actuators A Phys.*, vol. 179, pp. 17–31, 2012.

[6] P. Puangmali, K. Althoefer, L. D. Seneviratne, D. Murphy, and P. Dasgupta, "State-of-the-art in force and tactile sensing for minimally invasive surgery," *Sensors Journal, IEEE*, vol. 8, no. 4, pp. 371–381, 2008.

[7] E. P. Westebring – van der Putten, R. H. M. Goossens, J. J. Jakimowicz, J. Dankelman, E. P. der Putten, R. H. M. Goossens, J. J. Jakimowicz, J. Dankelman, E. P. Westebring – van der Putten, R. H. M. Goossens, J. J. Jakimowicz, and J. Dankelman, "Haptics in minimally invasive surgery-a review," *Minim. Invasive Ther. Allied Technol.*, vol. 17, no. 1, pp. 3–16, Jan. 2008.

[8] E. Vander Poorten, E. Demeester, P. Lammertse, E. V. B. Vander Poorten, E. Demeester, and P. Lammertse, "Haptic feedback for medical applications, a survey," *Proc. Actuator*, pp. 18–20, 2012.

[9] T. Yoneyama, T. Watanabe, H. Kagawa, J. Hamada, Y. Hayashi, and M. Nakada, "Force-detecting gripper and force feedback system for neurosurgery applications," *Int. J. Comput. Assist. Radiol. Surg.*, vol. 8, no. 5, pp. 819–829, Sep. 2013.

[10] Y. Kanada, T. Yoneyama, T. Watanabe, H. Kagawa, N. Sugiyama, K. Tanaka, and T. Hanyu, "Force Feedback Manipulating System for Neurosurgery," in *Procedia CIRP*, 2013, vol. 5, no. 1, pp. 133–136.

[11] Y. Fujihira, T. Hanyu, Y. Kanada, T. Yoneyama, T. Watanabe, and H. Kagawa, "Gripping Force Feedback System for Neurosurgery," *Int. J. Autom. Technol.*, vol. 8, no. 1, pp. 83–94, 2014.

[12] T. Takaki, Y. Omasa, I. Ishii, T. Kawahara, and M. Okajima, "Force visualization mechanism using a Moiré fringe applied to endoscopic surgical instruments," in *2010 IEEE International Conference on Robotics and Automation*, 2010, pp. 3648–3653.

[13] K. Tadano and K. Kawashima, "Development of 4-DOFs forceps with force sensing using pneumatic servo system," in *Robotics and Automation, 2006. ICRA 2006. Proceedings 2006 IEEE International Conference on*, 2006, pp. 2250–2255.

[14] D. Haraguchi, K. Tadano, and K. Kawashima, "A prototype of pneumatically-driven forceps manipulator with force sensing capability using a simple flexible joint," *IEEE Int. Conf. Intell. Robot. Syst.*, pp. 931–936, 2011.

[15] J. Peirs, J. Clijnen, D. Reynaerts, H. Van Brussel, P. Herijgers, B. Corteville, and S. Boone, "A micro optical force sensor for force feedback during minimally invasive robotic surgery," *Sensors Actuators A Phys.*, vol. 115, no. 2–3, pp. 447–455, 2004.

[16] M. Tada, S. Sasaki, and T. Ogasawara, "Development of an optical 2-axis force sensor usable in {MRI} environments," *Proceedings of IEEE Sensors*, vol. 2. pp. 984–989, 2002.

[17] M. Ohka, Y. Mitsuya, Y. Matsunaga, and S. Takeuchi, "Sensing characteristics of an optical three-axis tactile sensor under combined loading," *Robotica*, vol. 22, no. 2, pp. 213–221, Mar. 2004.

[18] K. Kamiyama, K. Vlack, T. Mizota, H. Kajimoto, K. Kawakami, and S. Tachi, "Vision-based sensor for real-time measuring of surface traction fields," *IEEE Comput. Graph. Appl.*, vol. 25, no. 1, pp. 68–75, Jan. 2005.

[19] C. Chorley, C. Melhuish, T. Pipe, and J. Rossiter, "Development of a tactile sensor based on biologically inspired edge encoding," in *Advanced Robotics, 2009. ICAR 2009. International Conference on*, 2009, pp. 1–6.

[20] T. Kawahara, S. Tanaka, and M. Kaneko, "Non-contact stiffness imager," *Int. J. Rob. Res.*, vol. 25, no. 5–6, pp. 537–549, May 2006.

[21] T. Fukuda, Y. Tanaka, M. Fujiwara, and A. Sano, "Softness measurement by forceps-type tactile sensor using acoustic reflection," in *2015 IEEE/RSJ International Conference on Intelligent Robots and Systems (IROS)*, 2015, pp. 3791–3796.

[22] T. Watanabe and Y. Fujihira, "Experimental investigation of effect of fingertip stiffness on friction while grasping an object," in *2014 IEEE International Conference on Robotics and Automation (ICRA)*, 2014, pp. 889–894.

[23] Y. Fujihira, K. Harada, T. Tsuji, and T. Watanabe, "Experimental investigation of effect of fingertip stiffness on resistible force in grasping," in *2015 IEEE International Conference on Robotics and Automation (ICRA)*, 2015, pp. 4334–4340.

[24] T. K. Kim, J. K. Kim, and O. C. Jeong, "Measurement of nonlinear mechanical properties of PDMS elastomer," *Microelectron. Eng.*, vol. 88, no. 8, pp. 1982–1985, Aug. 2011.

[25] N. Otsu, "A Threshold Selection Method from Gray-Level Histograms," *IEEE Trans. Syst. Man. Cybern.*, vol. 9, no. 1, pp. 62–66, 1979.

Tetsuyou Watanabe (M'02) received the B.S., M.S., and Dr.Eng. degrees in mechanical engineering from Kyoto University, Kyoto, Japan, in 1997, 1999, and 2003, respectively. From 2003 to 2007, he was a Research Associate with the Department of mechanical Engineering, Yamaguchi University, Japan. From 2007 to 2011, he was an assistant professor with Division of Human and Mechanical Science and Engineering, Kanazawa University. Since 2011, he has been an associate professor with Faculty of Mechanical Engineering, Institute of Science and Engineering, Kanazawa University. From 2008 to 2009, he was a visiting researcher at Munich University of Technology. His research interests include mechanics and control of robotic systems, medical sensors, surgical systems, grasping, object manipulation, and micro-manipulations.

Dr. Watanabe has received several awards, including the 2005 MAGDA Conference Best Paper Award from the Japan Society of Applied Electromagnetics and Mechanics, the 2008 Young Investigation Excellence Award from Robotics Society of Japan, the 2010 JSME Young Engineers Award from the Japan Society of Mechanical Engineers, and the 2012 SICE SI division conference excellent presentation Award.

Dr. Watanabe is a member of the IEEE Robotics and Automation Society and IEEE Engineering in Medicine & Biology Society. He is also a member of the Japan Society of Mechanical Engineers, the Robotics Society of Japan, the Japanese Society of Medical and Biological Engineering and the Society of Instrument and Control Engineers.

Takanobu Iwai received the B.S. and M.S. degrees in mechanical engineering from Kanazawa University, Kanazawa, Japan, in 2014 and 2016. His research interests include sensors, medical sensors, and surgical systems.

Toshio Koyama received the B.S. degree in mechanical engineering from Kanazawa University, Kanazawa, Japan, in 2015. His research interests include sensors, medical sensors, and surgical systems.

Takeshi Yoneyama received the B.S., M.S. and Dr. Eng. degrees in mechanical engineering from The University of Tokyo, in 1979, 1981 and 1984 respectively.

From 1984 to 1991, he was a Research Associate in the Department of Mechanical Engineering of Kanazawa University. From 1991 to 2001, he was an Associate Professor in the same department. From 2001 he has been a Professor in the school of Mechanical Engineering, Faculty of Mechanical Engineering, Institute of Science and Engineering, Kanazawa University. His research interests include sensors, machine design, surgical systems, sports engineering, production engineering for plastic deformation process, injection molding and composite material processes.

Prof. Yoneyama received several awards, including 2004 Education Award from the Japan Society of Mechanical Engineers, 2006 Best Paper Award from the Japan Society of Technology of Plasticity.

Prof. Yoneyama is a member of the Japan Society of Mechanical Engineers, the Japan Society of Technology of Plasticity, the Japan Society for Precision Engineering, Japanese Society for Medical and Biological Engineering